J|A|C|S
ARTICLES
Published on Web 01/26/2002

Dynamics of Energy Transfer in Peptide−Surface Collisions

Oussama Meroueh and William L. Hase*

Contribution from the Department of Chemistry, Wayne State University, Detroit, Michigan 48202-3489

Received August 16, 2001

Abstract: Classical trajectory simulations are performed to study energy transfer in collisions of protonated triglycine $(Gly)_3$ and pentaglycine $(Gly)_5$ ions with *n*-hexyl thiolate self-assembled monolayer (SAM) and diamond {111} surfaces, for a collision energy E_i in the range of 10−110 eV and a collision angle of 45°. Energy transfer to the peptide ions' internal degrees of freedom is more efficient for collision with the diamond surface; i.e., 20% transfer to peptide vibration/rotation at $E_i = 30$ eV. For collision with diamond, the majority of E_i remains in peptide translation, while the majority of the energy transfer is to surface vibrations for collision with the softer SAM surface. The energy-transfer efficiencies are very similar for $(Gly)_3$ and $(Gly)_5$. Constraining various modes of $(Gly)_3$ shows that the peptide torsional modes absorb ∼80% of the energy transfer to the peptide's internal modes. The energy-transfer efficiencies depend on E_i. These simulations are compared with recent experiments of peptide SID and simulations of energy transfer in $Cr(CO)_6^+$ collisions with the SAM and diamond surfaces.

I. Introduction

The development of ionization techniques[1−5] in combination with tandem mass spectrometry[6] has made it possible to study the gas-phase collision-induced dissociation (CID)[7] and surface-induced dissociation (SID)[8,9] of small peptides.[10−15] SID may be viewed as an extension of CID, in which the collider gas projectile is replaced by a surface. In a typical SID experiment,[8,9] an ion with a fixed incident angle θ_i and translational energy E_i is aimed at a surface. Upon collision with the surface, there is transfer of some of the ion's translational energy to the surface vibrations E_{surf} and the ion's internal degrees of freedom E_{int};

$$E_i = E_f + \Delta E_{surf} + \Delta E_{int} \quad (1)$$

where E_f is the ion's final translational energy after collision. This energy transfer model assumes that the collisions are electronically adiabatic and the excitation of electronic states of either the projectile or surface is unimportant. Such a model is consistent with experiments utilizing hydrocarbon surfaces, which do not have low-lying electronic states.[8,9,12−15]

SID has been used to extract important information about the structure and thermochemistry of various ions.[12−25] The internal energy distribution of the scattered ion $P(E_{int})$, in combination with RRKM modeling[14,26,27] and fragmentation efficiency curves, provides sufficient information to determine threshold energies for the ion's dissociation pathways,[14] if RRKM theory is a valid model for the ion's unimolecular dissociation.[28,29] Several methods have been developed to determine $P(E_{int})$,[30−32] though obtaining an accurate $P(E_{int})$

(1) Kulik, W.; Heerma, W. *Biomed. Environ. Mass Spectrom.* **1988**, *15*, 419.
(2) Leclerq, P.A.; Desiderio, D. M. O*rg. Mass Spectrom.* **1973**, *7*, 515.
(3) Milne, G. W. A.; Axenrod, T.; Fales, H. M. *J. Am. Chem. Soc.* **1970**, *92*, 5170.
(4) Tsang, C. W.; Harrison, A. G. *J. Am. Chem. Soc.* **1976**, *98*, 1301.
(5) Hillenkamp, F.; Karas, M.; Beavis, R. C.; Chait, B. T. *Anal. Chem.* **1991**, *63*, 1193A.
(6) Busch, K. L.; Glish, G. L.; McLuckey, S. A. *Mass Spectrometry/Mass Spectrometry*: *Techniques and Applications of Tandem Mass Spectrometry*; VCH Publishers: New York, 1988.
(7) Rodgers, M. T.; Armentrout, P. B. *J. Phys. Chem. A* **1997**, *101*, 1238.
(8) Cooks, R. G.; Ast, T.; Mabud, M. A. *Int. J. Mass Spectrom. Ion Processes* **1990**, *100*, 209.
(9) Mabud, M. A.; Dekrey, M. J.; Cooks, R. G. *Int. J. Mass Spectrom. Ion Processes* **1985**, *67*, 285.
(10) Marzluff, E. M.; Beauchamp, J. L. In *Large Ions: Their Vaporization, Detection and Structural Analysis*; Baer, T., Ng, C. Y., Powis, I., Eds.; John Wiley and Sons Ltd.: New York, 1996.
(11) Klassen, J. S.; Kerbale, P. *J. Am. Chem. Soc.* **1997**, *119*, 6552.
(12) Schultz, D. G.; Lim, H.; Garbis, S.; Hanley, L. *J. Mass Spectrom.* **1999**, *34*, 217.
(13) Dongré, A. R.; Jones, J. L.; Somogyi, À.; Wysocki, V. H. *J. Am. Chem. Soc.* **1996**, *118*, 8365.
(14) Laskin, J.; Denisov, E.; Futrell, J. *J. Am. Chem. Soc.* **2000**, *122*, 9703.
(15) Laskin, J.; Denisov, E.; Futrell, J. *J. Phys. Chem. B* **2001**, *105*, 1895.
(16) de Maaijer-Gielbert, J.; Somogyi, A.; Wysocki, V. H.; Kisemaker, P. G.; Weeding, T. L. *Int. J. Mass Spectrom.* **1988**, *174*, 81.
(17) Morris, M. R.; Riederer, D. E., Jr.; Winger, B. E.; Cooks, R. G.; Ast, T.; Chidsey, C. E. D. *Int. J. Mass. Spectrom. Ion Processes* **1992**, *122*, 181.
(18) Burroughs, J. A.; Wainhaus, S. B.; Hanley, L. *J. Phys. Chem.* **1994**, *98*, 10913.
(19) Burroughs, J. A.; Wainhaus, S. B,; Hanley, L. *J. Phys. Chem.* **1995**, *103*, 6706.
(20) Winger, B. E.; Laue, H.-J.; Horning, S. R.; Julian, R. K.; Lammert, S. A.; Riederer, D. E., Jr.; Cooks, R. G. *Rev. Sci. Instrum.* **1992**, *63*, 5613.
(21) Miller, S. A.; Riederer, D. E., Jr.; Winger, B. E.; Cooks, R. G.; Ast, T.; Chidsey, C. E. D. *Int. J. Mass Spectrom.. Ion Processes* **1992**, *122*, 181.
(22) Hayakawa, S.; Feng, B.; Cooks, R. G. *Int. J. Mass Spectrom.* **1997**, *167*, 525.
(23) Wainhaus, S. B.; Gislason, E. A.; Hanley, L. *J. Am. Chem. Soc.* **1997**, *119*, 4001.
(24) Vékey, K.; Somogyi, À; Wysocki, V. H. *J. Mass. Spectrom.* **1995**, *30*, 212.
(25) de Maaijer-Gilbert, J.; Beijersbergen, J. H. M.; Kistemaker, P. G.; Weeding, T. L. *Int. J. Mass Spectrom. Ion Processes* **1996**, *153*, 119.
(26) Rodgers, M. T.; Ervin, K. M.; Armentrout, P. B. *J. Chem. Phys.* **1997**, *106*, 4499.
(27) Beck, R. D.; Rockenberger, J.; Weis, P.; Kappes, M. M. *J. Chem. Phys.* **1996**, *104*, 3638.
(28) Bunker, D. L.; Hase, W. L. *J. Chem. Phys.* **1973**, *59*, 4621.
(29) Baer, T.; Hase, W. L. *Unimolecular Reaction Dynamics: Theory and Experiments*; Oxford University Press: New York, 1996.
(30) (a) Vékey, K.; Brenton, A. G.; Beynon, J. H. *J. Phys. Chem.* **1986**, *90*, 3569. (b) Wysocki, V. H.; Kenttämaa, H. I.; Cooks, R. G. *Int. J. Mass Spectrom. Ion Processes* **1987**, *75*, 181.

10.1021/ja011987n CCC: $22.00

remains a difficult endeavor. Experiments indicate that the energy transferred to the ion depends on several factors which include the surface composition,[16,17,33,34] the projectile structure,[12] the collision energy E_i,[18,35,36] and the incident angle θ_i.[18,35,37] Work by Kubišta et al.[31] suggests that the fraction of E_i transferred to ion internal excitation may be independent of θ_i.

The internal energy distribution of the scattered ion, along with the ion's final translational energy E_f and the energy deposited in the surface vibrations ΔE_{surf}, may be determined from classical trajectory simulations.[35−39] Recent simulations[39] of the surface-induced dissociation of $Cr(CO)_6^+$ ions on diamond {111} and *n*-hexyl thiolate self-assembled monolayer (SAM) surfaces give efficiencies of 30, 14, and 56% and 10, 69, and 21%, respectively, for energy transfer to E_{int}, E_{surf}, and E_f. However, the energy-transfer dynamics of peptide SID may be different from that of $Cr(CO)_6^+$, since peptides have low-frequency torsional motions which are very important for the transfer of energy to ion vibration.[40]

Several studies have investigated the dynamics of peptide collisional activation.[6,12−15,41,42] Trajectory simulations of protonated $(Gly)_n$ and $(Ala)_n$, $n = 1-7$, collision-induced dissociation (CID) show that the energy-transfer efficiency depends on both the peptide structure and collision energy.[42] Though the simulations show that the amount of energy transferred to peptide rotation is much smaller than that transferred to peptide vibration, linear peptides are more rotationally excited than are folded, more compact peptides. From peptide SID experiments on a hydrogenated self-assembled monolayer, Schultz et al.[12] determined that the average E_f is 24% of the incident energy for protonated $(Gly)_3$ and $(Gly)_4$. Average E_f values of 21 and 17% of the collision energy were found for a cyclic dipeptide and a four-membered ring peptide, respectively.[12] Assuming a 17% $E_i \rightarrow E_{surf}$ energy-transfer efficiency obtained from work on benzene SID,[43] they estimated a 59−66% $E_i \rightarrow E_{surf}$ efficiency and a broad distribution for E_f. In recent experiments, Laskin et al.[14,15] studied protonated $(Ala)_2$ SID in collisions with a fluorinated SAM. They found a relatively narrow distribution of E_{int} with an average ΔE_{int} 21% of the collision energy.

In this article, quasiclassical trajectory simulations are reported of the energy-transfer dynamics associated with the scattering of protonated polyglycine $(Gly)_3$ and $(Gly)_5$ peptide ions off diamond {111} and *n*-hexyl thiolate SAM surfaces. The diamond and SAM surfaces represent stiff and soft hydrogenated surfaces,[39] respectively. Previous work[42] has shown that the energy-transfer dynamics is dependent on the intermolecular potential between the projectile and the surface, and ab initio calculations are performed to determine an accurate analytic potential energy function for the interaction between peptide ions and hydrogenated hydrocarbon surfaces. These ab initio calculations are based on small molecules, which represent the atoms and functional groups of the peptides, and methane, which represents the hydrogen and carbon atoms of the diamond and SAM surfaces. A comparison is made of the energy-transfer dynamics for both extended and folded structures of protonated $(Gly)_3$ colliding with the diamond and SAM surfaces. The simulations are performed at a collision energy E_i of 30 eV and collision angle θ_i of 45°, and they show how the transfer of E_i to E_{int}, E_{surf}, and E_f depends on the surface stiffness and peptide structure. Trajectory simulations are also carried out for the scattering of folded $(Gly)_3$ and $(Gly)_5$ peptides on the diamond {111} surface to study the role of the peptide size on the energy-transfer dynamics. Further trajectory simulations are carried out for the collision of folded $(Gly)_3$ with the diamond surface at E_i =10, 70, and 110 eV to study the effect of the collision energy on the energy transfer. Previous work on the gas-phase collisional activation of small peptides[42] has shown that the most of the internal energy absorbed by the peptide is transferred to its torsions. A similar study is carried out here in which the stretching and bending motions of the peptide are constrained to study the internal energy-transfer pathways in peptide surface scattering. Finally, the simulations reported here, of the energy transfer in peptide SID, are compared with previous simulations of $Cr(CO)_6^+$ SID on the diamond {111} and SAM surfaces[39] and energy transfer in collisions of protonated polyglycine and polyalanine peptide ions with argon.[42]

II. Potential Energy Function

The general analytic potential energy function used for the peptide/diamond {111} and peptide/*n*-hexyl thiolate SAM systems is given by

$$V = V_{peptide} + V_{surface} + V_{peptide,surface} \quad (2)$$

when $V_{peptide}$ is the peptide protonated intramolecular potential, $V_{surface}$ is the potential for either the diamond or SAM surface, and $V_{peptide,surface}$ is the peptide/surface intermolecular potential. Each of these potential terms is described below.

A. Peptide Potential. The potentials for the polyglycine peptides $(Gly)_3$ and $(Gly)_5$ are represented by the AMBER valence force field of Cornell et al.[44] and expressed as

$$V_{peptide} = \sum_{bonds} K_r(r - r_{eq})^2 + \sum_{angles} K_\theta(\theta - \theta_{eq})^2 + \sum_{dihedrals} \frac{V_n}{2}[1 - \cos(n\phi - \gamma)] + \sum_{i>j} \left[\frac{A_{ij}}{r_{ij}^{12}} - \frac{B_{ij}}{r_{ij}^{6}} + \frac{q_i q_j}{r_{ij}}\right] \quad (3)$$

Conformers used in this study for the $(Gly)_3$ and $(Gly)_5$ peptides are shown in Figures 1 and 2, respectively. The folded structures were found using the SYBYL package (version 6.5, Tripos Associates, Inc., St. Louis, MO) via a simulated annealing procedure, which consisted of heating the molecule to $T_i = 500$ K for 1.5 ps and subsequently cooling the molecule to $T_f =$ 300 K for a period of 1 ps via an exponential cooling schedule.

(31) Kubista, J.; Dolejsek, Z.; Herman, Z. *Eur. Mass Spectrom*, **1998**, *4*, 311.
(32) Laskin, J.; Byrd, M.; Futrell, J. *Int. J. Mass Spectrom.* **2000**, *195/196*, 285.
(33) Hakansson, K.; Axelsson, J.; Palmblad, M.; Hakansson, P. *J. Am. Soc. Mass Spectrom.* **2000**, *11*, 210.
(34) Wainhaus, S. B.; Lim, H.; Schultz, D. G.; Hanley, L. *J. Am. Chem. Soc.* **1997**, *106*, 110329.
(35) Schultz, D. G.; Wainhaus, S. B.; Hanley, L.; de Sainte Claire, P.; Hase, W. L. *J. Chem. Phys.* **1997**, *106*, 10337.
(36) Schultz, D. G.; Hanley, L. *J. Chem. Phys.* **1988**, *109*, 10976.
(37) Hanley, L.; Lim, L. H.; Schultz, D. G.; Wainhaus, S. B.; de Sainte Claire, P.; Hase, W. L. *Nucl. Instrum. Methods Phys. Res. B* **1997**, *125*, 218.
(38) Bosio, S. B. M.; Hase, W. L. *Int. J. Mass Spectrom.* **1998**, *174* , 1.
(39) Meroueh, O.; Hase, W. L. *Phys. Chem. Chem. Phys.* **2001**, *3*, 2306.
(40) Meroueh, O.; Hase, W. L. *Int. J. Mass Spectrom.* **2000**, *201*, 233.
(41) Marzluff, E. M.; Campbell, S.; Rodgers, M. T.; Beauchamp, J. L. *J. Am. Chem. Soc.* **1994**, *116*, 7787.
(42) Meroueh, O.; Hase, W. L *J. Phys. Chem. A* **1999**, *103*, 3981.
(43) Vékey, K.; Somogyi, Á.; Wysocki, V. H. *Rapid Commun. Mass Spectrom.* **1996**, *10*, 911.
(44) Cornell, W. D.; Cieplak, P.; Bayley, C. I.; Gould, I. R.; Merz, K. M.; Ferguson, D. M.; Spellmeyer, D. C.; Fox, T.; Caldwell, J. W.; Kollman, P. A. *J. Am. Chem. Soc.* **1995**, *117*, 5179.

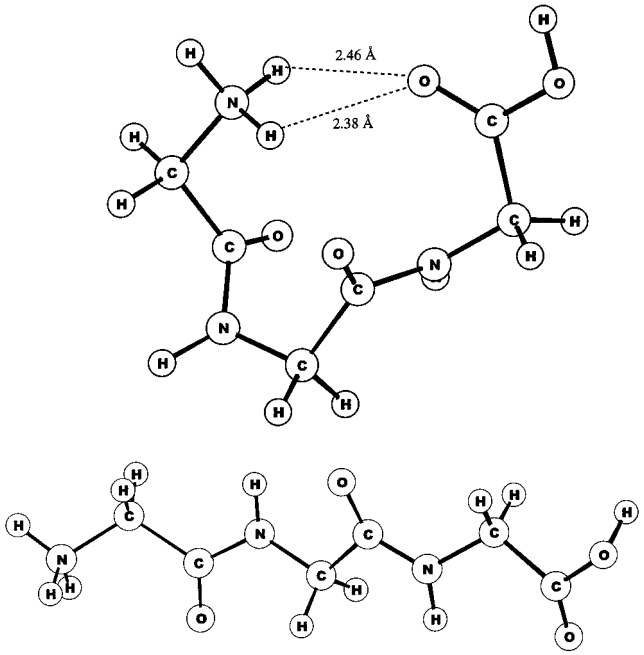

Figure 1. Folded and extended protonated $(Gly)_3$ peptide models used in this study. The dashed lines denote important hydrogen bond ineractions.

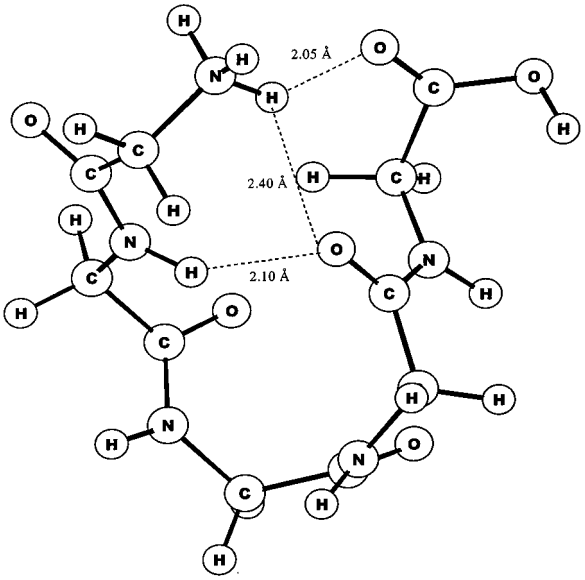

Figure 2. Folded protonated $(Gly)_5$ peptide model used in this study. The dashed lines denote important hydrogen bond interactions.

Once the conformer was found, a local energy minimization procedure using the VENUS[45] package was carried out, until a potential energy minimum was found. The extended structure of $(Gly)_3$ was found by a local energy minimization of a $(Gly)_3$ β-sheet structure. Favorable hydrogen-bonding interactions, which stabilize the folded conformers, are shown in the figures.

B. Surface Potentials. For the simulations reported here, the same model was used for the diamond {111} surface as used previously[39] to simulate $Cr(CO)_6^+$ SID (i.e., see Figure 1 in ref 39), except the surface was enlarged to 32 Å × 34 Å so that collisions of the peptide ions with the surface were accurately represented. The surface model is hydrogen terminated, with four layers of carbon atoms, and has a thickness of 8.0 Å from the top hydrogen atoms to the bottom carbon atoms. Massive atoms were attached to the bottom corner atoms of the model, via harmonic potentials with large force constants, to ensure the model did not move when struck by the peptide ions. The potential energy function for the diamond {111} model consists of harmonic stretches and bends, with force constants chosen to fit the diamond phonon spectrum.[46]

The same model for the *n*-hexyl thiolate SAM, developed previously[39] for $Cr(CO)_6^+$ SID, was used here, since the model is sufficiently large to represent collisions of the $(Gly)_3$ and $(Gly)_5$ peptide ions. The potential energy function for the SAM is based on the Mar−Klein potential[47] for alkanethiolates, with the constraints of the C−H and C−C stretches and C−H bends removed and the addition of more accurate short-range repulsive interactions between the atoms of the SAM. The latter is required so that the potential of the SAM is accurately described when the SAM is compressed by the projectile collisions. These accurate short-range repulsive interactions were determined from ab initio calculations.[39] The analytic potential energy function and parameters for the SAM model and a depiction of the model are given in ref 39.

C. Peptide/Surface Potential. As shown in previous simulations of peptide CID,[42] accurate repulsive potentials between the colliding peptide ion and the surface are necessary to accurately describe energy transfer in peptide SID. Such potentials have not been developed for peptide ions interacting with hydrocarbon surfaces such as diamond {111} and alkyanethiolate SAMs, and they were derived here from ab initio calculations. The peptide/surface intermolecular potential is modeled by a sum of two-body potentials between the atoms of the peptide and surface. The two-body potential is given by

$$V_{XY} = A_{XY}\exp(-B_X Y r_{ij}) + C_{XY}/r_{ij}^{\,6} \qquad (4)$$

where X corresponds to C or H atoms of the diamond or SAM surface and Y corresponds to H, C, O, or N atoms of the peptide.

To determine the parameters for the above two-body potentials, ab initio potential energy curves were calculated between CH_4, as a model for the C and H atoms of the diamond {111} and *n*-hexyl thiolate SAM surfaces, and CH_4, NH_3, NH_4^+, H_2CO, and H_2O, as models for the different types of atoms and functional groups comprising the polyglycine peptides. The ab initio calculations are carried out at the MP2 level of theory with the frozen-core approximation. The molecules are first optimized at the MP2 level of theory using as a single-ζ core and triple-ζ valence representation 6-311+g(2df,2pd) basis set, which includes a set of diffuse s- and p-type Gaussian functions on heavy atoms and three sets of d functions and one set of f functions for first-row atoms and 2 sets of p functions and one set of d functions for hydrogen atoms. The molecules are held fixed in these optimized geometries and intermolecular potential energy curves for different orientations of the CH_4/CH_4, CH_4/NH_3, CH_4/NH_4^+, CH_4/H_2CO, and CH_4/H_2O systems are calculated via the supermolecular approach[48] with the above basis

(45) Hase, W. L.; Duchovic, R. J.; Hu, X.; Komornicki, A.; Lim, K. F.; Lu, D.-h; Peslherbe, G. H.; Swamy, K. N.; Vande Linde, S. R.; Zhu, L.; Varandas, A.; Wang, H.; Wolf, R. J. *QCPE* **1996**, *16*, 671.
(46) Hass, K. C.; Tamor, M. A.; Anthony, T. R.; Banholzer, W. F. *Phys. Rev. B* **1992**, *45*, 7171.
(47) Mar, W.; Klein, M. *Langmuir* **1994**, *10*, 188.
(48) van Duijneveldt, F. B. In *Basis Set Superposition Error*, Schreiner, S., Ed.; John Wiley & Sons Ltd.: West Sussex, U.K., 1997; p 81.

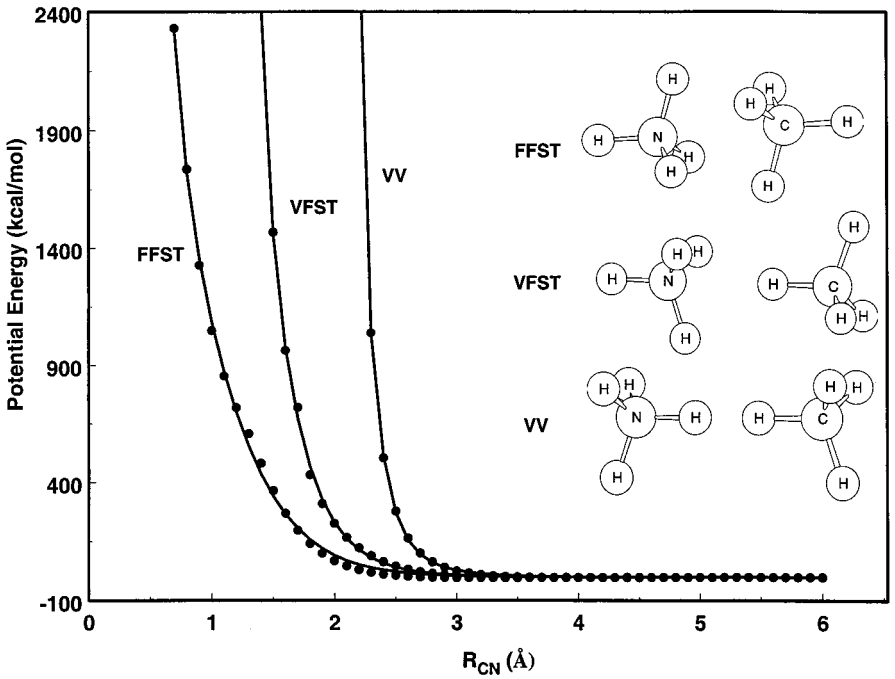

Figure 3. Fitted analytic potential energy function compared to ab initio data (●) for the CH_4/NH_4^+ system.

set and full-counterpoise corrections.[49−52] All of the ab initio calculations are carried out with the GAUSSIAN 98 suite of programs.[53]

The calculated ab initio potential energy curves for the CH_4/NH_4^+ system are shown in Figure 3. The curves for the different orientations of a particular system were fit simultaneously by a sum of the two-body functions in eq 4. The fitting was accomplished by nonlinear least squares. The fits to the potential energy curves for the other systems are similar to the one in Figure 3. The potential energy parameters derived from the fits are listed in Table 1.

III. Computational Procedure

The classical trajectory[54−56] simulations were carried out with the general chemical dynamics package VENUS.[45] Initial conditions for the trajectories were chosen to model experiments. The center of a beam of peptide ion projectiles is aimed at the center of the surface, with fixed incident angle θ_i and fixed initial translational energy E_i. The radius of the beam was chosen so that the beam overlapped a unit area on the surface, and the trajectory results are insensitive to its radius. Following the procedure described previously,[38,57] the peptide projectile for each trajectory was randomly placed in the cross section of this beam and randomly rotated about its center of mass so that it has an initial random orientation with respect to the surface. The azimuthal angle χ, between the beam and a fixed plane perpendicular to the surface, was sampled randomly between 0 and 2π. Such a random sampling of χ simulates collisions with different domains of growth on the SAM and diamond surfaces.[57] The distance between the center of the beam and the center of the top of the surface was set to 30 Å.

Table 1. Parameters for Two-Body Potential Energy Function in Eq 4

$X–Y^a$	$A_{XY}{}^b$	$B_{XY}{}^c$	$C_{XY}{}^d$
		CH_4/CH_4	
C−C	20604	6.1940	21.873
C−H	12455	3.3143	0.18877
H−H	3485.1	8.8492	0.00097365
		CH_4/NH_4^+	
C−N	26572	7.4777	72.3877
C−H	10189	3.0839	2.9818
H−N	5469.5	3.9466	0.59338
H−H	3923.4	8.5594	0.00038714
		CH_4/NH_3	
C−N	2320.1	2.7989	82.024
C−H	3139.4	2.4881	84.804
H−N	5166.0	4.2389	0.7863
H−H	3244.0	7.5592	0.0011701
		CH_4/H_2CO^e	
C−C	84389	5.5696	6516.4
C−O	4071.1	2.2660	74.611
H−C	6808.4	4.6973	0.67710
H−O	4366.7	5.9569	0.00049008
		CH_4/H_2O	
C−O	75068	6.0169	0.22928
C−H	14817	3.6565	32.142
H−O	4986.9	2.9871	13.444
H−H	4390.9	9.5165	0.00014392

[a] *X* is an atom of the first molecule, CH_4, and *Y* is an atom of the second molecule. [b] Units are kcal/mol. [c] Units are 1/Å. [d] Units are kcal Å^6/mol. [e] The H−H interaction is assumed to be the same as that for the CH_4/CH_4 system.

(49) Boys, S. F.; Bernardi, F. *Mol. Phys.* **1970**, *19*, 553.
(50) Duijneveldt, F. B. v.; Duijneveldt, H. G. C. v.; Rijdt, J. H. D. *Chem. Rev.* **1994**, *94*, 1873.
(51) Newton, M. D.; Kestner, N. R. *Chem. Phys. Lett.* **1983**, *94*, 198.
(52) Xantheas, S. S. *J. Chem. Phys.* **1996**, *104*, 1873.
(53) Frisch, M. J.; Trucks, G. W.; Schlegel, H. B.; Scuseria, G. E.; Robb, M. A.; Cheeseman, J. R.; Zakrzewski, V. G.; Montgomery, J. A.; Stratmann, R. E.; Burant, J. C.; Dapprich, S.; Millam, J. M.; Daniels, A. D.; Kudin, K. N.; Strain, M. C.; Farkas, O.; Tomasi, J.; Barone, V.; Cossi, M.; Cammi, R.; Mennucci, B.; Pomelli, C.; Adamo, C.; Clifford, S.; Ochterski, J.; Petersson, G. A.; Ayala, P. Y.; Cui, Q.; Morokuma, K.; Malick, D. K.; Rabuck, A. D.; Raghavachari, K.; Foresman, J. B.; Cioslowski, J.; Ortiz, J. V.; Stefanov, B. B.; Liu, G.; Liashenko, A.; Piskorz, P.; Komaromi, I.; Gomperts, R.; Martin, R. L.; Fox, D. J.; Keith, T.; Al-Laham, M. A.; Peng, C. Y.; Nanayakkara, A.; Gonzalez, C.; Challacombe, M.; Gill, P. M. W.; Johnson, B. G.; Chen, W.; Wong, M. W.; Andres, J. L.; Head-Gordon, M.; Replogle, E. S.; Pople, J. A. *Gaussian 98 and Revision A.7*; Gaussian Inc.: Pittsburgh, PA, 1998.
(54) Bunker, D. L. *Methods Comput. Phys.* **1971**, *10*, 287.
(55) Bunker, D. L. *Acc. Chem. Res.* **1974**, *7*, 195.
(56) Peslherbe, G. H.; Wang, H.; Hase, W. L. In *Advances in Chemical Physics*; Ferguson, D., Siepmann, J. I.. Truhlar, D. G., Eds.; Wiley: New York, 1999; Vol. 105, p 171.
(57) Bosio, S. B. M.; Hase, W. L. *J. Chem. Phys.* **1997**, *107*, 9677.

Table 2. Average Energy (%) Transferred to Peptide Internal Energy, Surface Vibrations, and Peptide Translations for Folded and Extended Protonated $(Gly)_3$ Collisions with the Diamond and SAM Surfaces[a]

	diamond		SAM	
	folded	extended	folded	extended
ΔE_{int}	18	20	7	8
ΔE_{surf}	9	8	63	54
E_f	73	72	30	38

[a] The collision energy and angle are 30 eV and 45°, respectively.

The initial conditions for the vibrational modes of the peptides were chosen via the quasiclassical normal-mode method,[56,58−60] which includes zero-point energies. Excess energies, for each normal mode of vibration, were selected from the mode's 300 K harmonic oscillator Boltzman distribution.[60] The energy was randomly partitioned between kinetic and potential by choosing a random phase for each normal mode.[58] A 300 K rotational energy of *RT*/2 was added to each principal axis of rotation of the projectile.

Initial conditions for the surfaces were chosen by assigning velocities, sampled from a Maxwell−Boltzmann distribution at 300 K, to the surface atoms. The surfaces were then equilibrated for 2 ps of molecular dynamics by scaling the velocities[61] so the temperature corresponds to that for a 300 K classical Boltzmann distribution. The structure obtained from this equilibration process is then used as the initial structure for a 0.1-ps equilibration run at the beginning of each trajectory. A time step of 0.1 fs was used to integrate the classical equations of motion, to ensure conservation of energy to eight significant figures.

Three hundred trajectories were computed for each set of initial conditions with fixed E_i and θ_i. When the trajectory is terminated, the projectile's internal energy change ΔE_{int} is determined by subtracting the initial value of the projectile's internal energy from its final value. The energy transferred to the surface ΔE_{surf} is then determined from the energy conservation relationship in eq 1.

IV. Trajectory Results

A. Effects of Surface Stiffness and Peptide Structure. Values for the average percent energy transferred to peptide internal energy, surface vibrations, and peptide translation for folded and extended $(Gly)_3$ collisions with the diamond and SAM surfaces are given in Table 2. The collisions are for an initial energy E_i of 30 eV and collision angle of 45°. Overall, the peptide structure does not have a strong effect on the manner in which the energy transfer is partitioned, particularly for collisions with the diamond surface. For collision with the SAM surface, the transfer of energy to E_{int} is unaffected by the peptide structure; however, there is a 9% decrease and increase of energy transferred to E_{surf} and E_f, respectively, for the extended $(Gly)_3$.

The surface has a pronounced effect on how the energy is transferred. For collision with the diamond surface, more than 70% of the energy remains in peptide translation, while for collision with the SAM surface, more than 50% of the energy is transferred to surface vibrations. Approximately 20% of the energy is transferred to the peptide vibrational/rotational degrees of freedom upon collision with diamond, which is 2−3 times larger than for collision with the SAM. Only a small fraction of the energy transferred to the ion's internal modes is rotation. For extended and folded $(Gly)_3$ collisions with diamond, 15 and 12% of the energy transferred to E_{int} is to rotation, respectively, while for collision with the SAM these values are both 8%.

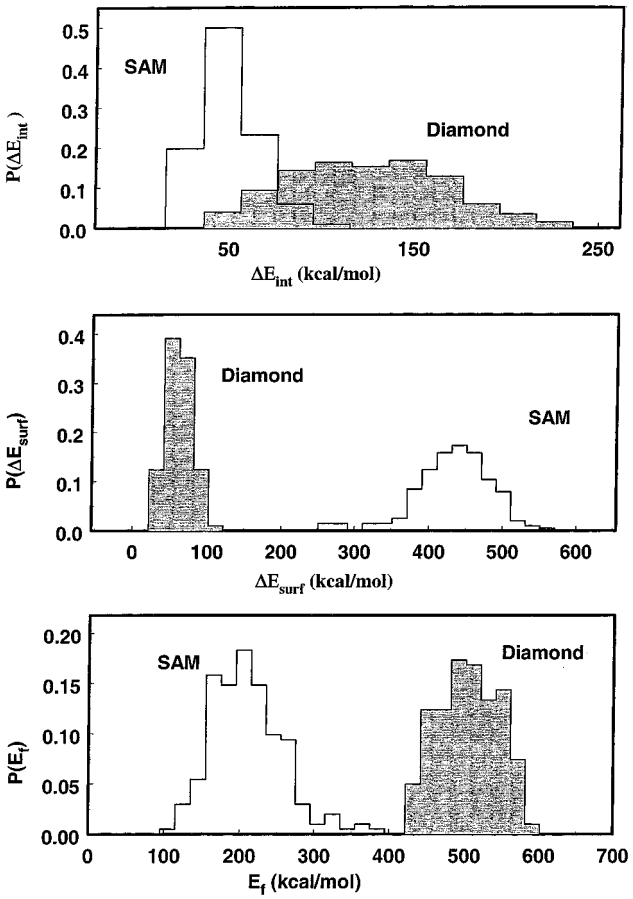

Figure 4. Distribution of the energy transfer to the ion (ΔE_{int}) and to the surface (ΔE_{surf}) and the translational energy of the recoiling ion (E_f) as a result of folded $(Gly)_3-H^+$ collisions with the diamond and SAM surfaces at an initial translational energy of 30 eV (692 kcal/mol) and θ_i of 45°.

Distributions of the energy transfers are similar for extended and folded $(Gly)_3$ and are shown in Figure 4 for the folded structure. The diamond and SAM surfaces give similar $P(E_f)$ distributions similar in shape, but much different $P(\Delta E_{int})$ and $P(\Delta E_{surf})$ distributions. $P(\Delta E_{int})$ is significantly broader for collision with diamond as compared to the SAM surface.

B. Energy-Transfer Pathways. Peptide ions have a hierarchy of vibrational modes ranging from high-frequency stretches to low-frequency torsions. It is of interest to determine which types of peptide modes are most efficiently excited by collisional activation. In a previous simulation[40] of exciting extended $(Gly)_4$ by zero impact parameter collisions with Ar atoms at $E_i = 100$ kcal/mol, the role of different types of modes on the energy transfer was investigated by increasing the mode frequencies to the high-frequency limit at which the modes are constrained and do not accept energy. With none of the vibrations constrained, 58% of E_i is adsorbed by the peptide's internal degrees of freedom. When all of the modes are constrained, except the torsions, this is lowered to 49%, which indicates that the torsions absorb ~84% of the internal energy transferred to the peptide.

As discussed above, with none of the folded $(Gly)_3$ modes constrained, 18, 9, and 73% of $E_i = 30$ eV is transferred to E_{int}, E_{surf}, and E_f, respectively, for collision with the diamond surface. With all of the modes of the $(Gly)_3$ peptide, except the

(58) Chapman, S.; Bunker, D. L. *J. Chem. Phys.* **1975**, *62*, 2890.
(59) Sloane, C. S.; Hase, W. L. *J. Chem. Phys.* **1977**, *66*, 1523.
(60) Cho, Y. J.; Vande Linde, S. R.; Zhu, L.; Hase, W. L. *J. Chem. Phys.* **1992**, *85*, 958.
(61) Allen, M. P.; Tildesley, D. J. *Computer Simulation of Liquids*; Oxford University Press Inc.: New York, 1987.

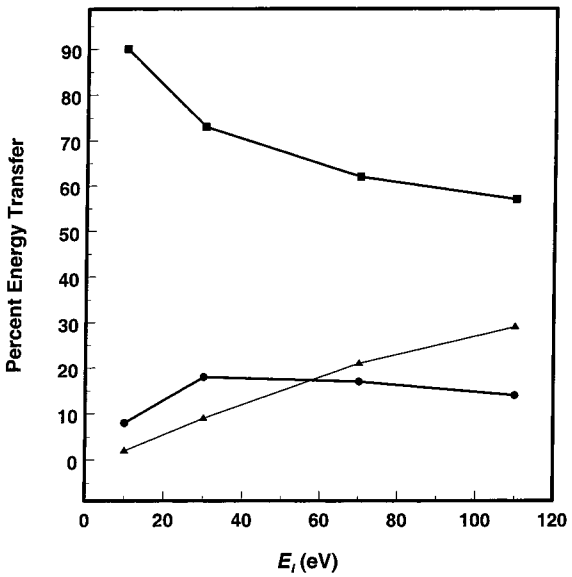

Figure 5. Percent energy transfer to E_{int} (●), E_{surf} (▲), and E_f (■) versus collision energy, for collisions of folded protonated $(Gly)_3$ with diamond {111} at $\theta_i = 45°$.

torsions, constrained as described above, these respective values become 14, 16, and 70%. Thus, as found in the previous simulation of peptide CID, ~80% of the internal energy transferred to the peptide in SID goes to the torsions.

C. Effect of Peptide Size. The effect of peptide size on the energy transfer was investigated by simulating collisions of folded $(Gly)_5$ with diamond at $E_i = 30$ eV and $\theta_i = 45°$. The results may be compared with those above for folded $(Gly)_3$. For folded $(Gly)_5$, the energy transfers of E_i to E_{int}, E_{surf}, and E_f are 23, 5, and 72%, respectively, which are only slightly different from the above respective values of 18, 9, and 73% for folded $(Gly)_3$. For $(Gly)_5$, as compared to $(Gly)_3$, there is a small 5% increase in $E_i \rightarrow E_{int}$ at the expense of $E_i \rightarrow E_{surf}$.

D. Effect of E_i. The initial peptide translational energy is expected to affect the energy-transfer dynamics, and this property was investigated by simulating collisions of folded $(Gly)_3$ with diamond {111} at E_i of 10, 70, and 110 eV, to complement the above results for $E_i = 30$ eV. The energy transfers for all the E_i are shown in Figure 5. It is seen that the energy transfer to the peptide increases from 8 to 18%, when E_i is increased from 10 to 30 eV, but then decreases as E_i is increased from 70 to 110 eV. Energy transfer to E_f decreases as E_i is increased. At high E_i , energy transfer to the diamond surface vibrations becomes more important than energy transfer to the peptide's vibrations.

E. Collision Lifetimes. The average lifetime[62,63] for the collision of folded $(Gly)_3$ with diamond {111}, at E_i of 10, 30, 70, and 110 eV, was studied by determining the average change in the $(Gly)_3$ vibrational and rotational energy versus time for the ensemble of trajectories calculated at each E_i. The results are shown in Figure 6. As E_i is increased, the collision lifetime becomes shorter. Since the collisions are direct, with no trapping of the peptide on the diamond surface, a simple model would assume the collision lifetime to be proportional to the collision velocity, which is proportional to $(E_i)^{1/2}$. The results in Figure 6 are only qualitatively consistent with such a model. Comparing

Table 3. Comparisons of Trajectory Simulations of Energy Transfer (%) for Folded Protonated $(Gly)_3$ and $Cr(CO)_6^+$ Collisions with Diamond {111}[a]

	ΔE_{int}		ΔE_{surf}		E_f	
E_i[b]	$(Gly)_3$	$Cr(CO)_6^+$	$(Gly)_3$	$Cr(CO)_6^+$	$(Gly)_3$	$Cr(CO)_6^+$
5		20		1		79
10	8		2		89	
30	18	30	9	14	73	56
70	17	17	21	29	62	54
110	14	16	29	38	57	46

[a] The collision angle is 45°. [b] The collision energy in eV.

Figures 5 and 6 shows that as E_i is increased the collision lifetime decreases and the energy transfers to peptide translation and peptide and surface vibrations decrease and increase, respectively.

V. Comparison of Peptide and $Cr(CO)_6^+$ Energy Transfer Dynamics

In recent work,[39,64] we have simulated the energy-transfer dynamics associated with $Cr(CO)_6^+$ SID and it is of considerable interest to compare the results of this work with that reported here for peptide SID. An important finding from these studies are the different energy transfers for $Cr(CO)_6^+$ and the protonated $(Gly)_3$ and $(Gly)_5$ peptide ions, with overall more efficient activation of the internal vibrational modes for the smaller projectile $Cr(CO)_6^+$. For $Cr(CO)_6^+$ collision with the SAM surface, at $E_i = 30$ eV and $\theta_i = 45°$, the energy transfers to E_{int}, and E_{surf}, and E_f are 10, 69, and 21%, respectively. For folded $(Gly)_3$ collision with the SAM, at the same E_i and θ_i, the respective values are 7, 63, and 30%, while for extended $(Gly)_3$ they are 8, 54, and 38%. The $Cr(CO)_6^+$ collisions transfer more energy to E_{int} and E_{surf} and less to E_f.

As shown in Table 3, more extensive comparisons between the $Cr(CO)_6^+$ and folded protonated $(Gly)_3$ ion energy-transfer dynamics may be made for collisions with diamond {111}. For all E_i, the $Cr(CO)_6^+$ collisions transfer more energy to E_{surf} and less to E_f than do the $(Gly)_3$ collisions. At low E_i, the energy transfer to E_{int} is larger for $Cr(CO)_6^+$ than $(Gly)_3$. However, at large E_i, the internal activation is similar for the two ions.

Though $(Gly)_3$ has more vibrational modes than does $Cr(CO)_6^+$, i.e., 69 versus 33, this does not necessarily translate into more efficient activation of the peptide. As shown above, by constraining the modes of the peptide,[40] only the peptide torsions are efficiently excited by collisional activation. Including the N−C−OH torsion, $(Gly)_3$ has nine torsional modes. For $Cr(CO)_6^+$ activation, only the six high-frequency CO stretch modes appear to be inactive to the reception of energy.[64] Folded $(Gly)_5$ has 15 torsional modes, and for its collisions with diamond {111}, the energy transfer to E_{int} is 23% for $E_i = 30$ eV, a value intermediate of the 18% for $(Gly)_3$ and 30% for $Cr(CO)_6^+$.

Besides identifying the number and types of projectile molecular modes that receive energy, the relative partitioning of the collision energy between the projectile modes, the surface vibrations, and projectile final translation depends on the relationships between the time scales for projectile vibration, surface vibration, and projectile translation.[65−67] The results in Table 3 show that at low E_i the higher frequency diamond modes

(62) Bernshtein, V.; Lim, K. F.; Oref, I. *J. Chem. Phys.* **1995**, *99*, 4531.
(63) Oref, I.; Bernshtein, V. *J. Chem. Phys.* **1998**, *108*, 3543.
(64) Meroueh, O.; Song, K.; Hase, W. L. *J. Phys. Chem. B*, submitted.
(65) Mahan, B. H. *J. Chem. Phys.* **1970**, *52*, 5221.

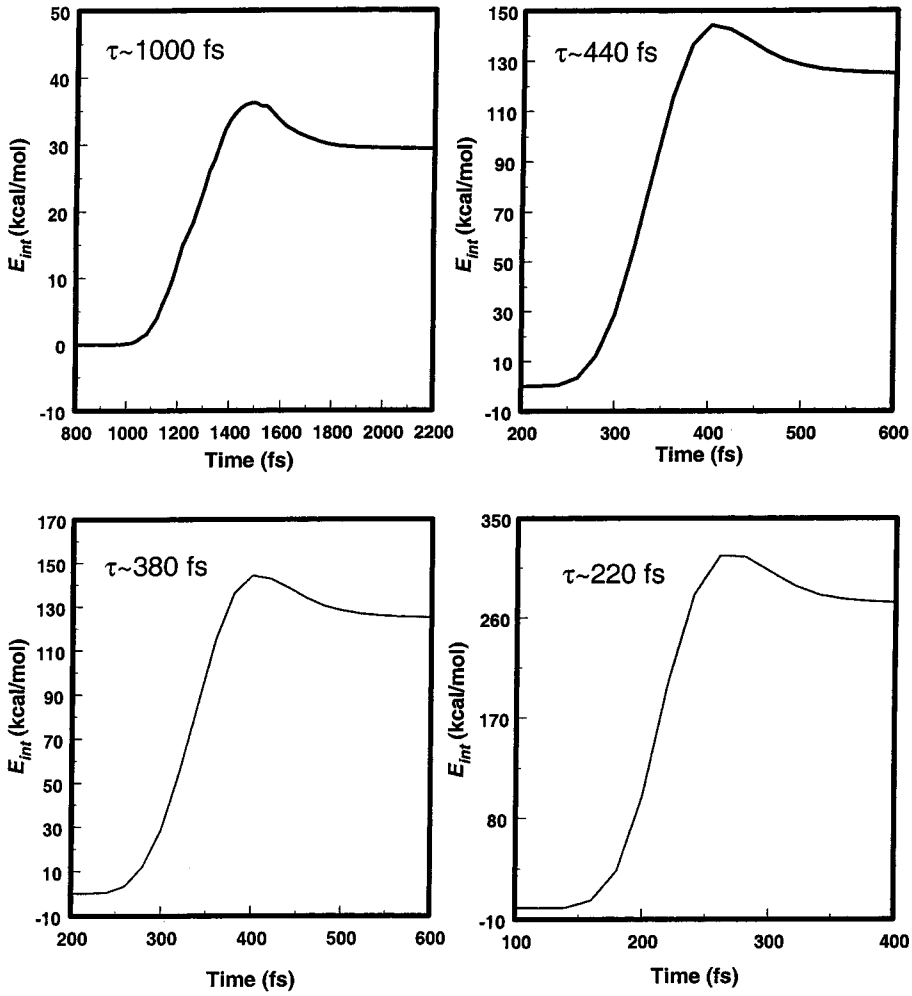

Figure 6. Ensemble average of the internal energy of folded $(Gly)_3$ versus time for $E_i = 10$ (upper left), 30 (upper right), 70 (lower left), and 110 eV (lower right). An estimate of the collision lifetime is shown in each graph.

are inactive and receive very little of the collision energy. However, as E_i is increased, the time scales for projectile translation and surface vibration become in accord and more energy is transferred to surface vibration at the expense of the scattered projectile's translation. A reflection of the change in the relationships between the different time scales, as E_i is increased, is the peak in the percent energy transfer to the projectile at E_i of ~30 eV, which is more pronounced for $Cr(CO)_6^+$ (See Table 3).

VI. Summary

The following are the important findings, from the simulations reported here, of 10−110-eV collisions of protonated polyglycine $(Gly)_3$ and $(Gly)_5$ ions with *n*-hexyl thiolate SAM and diamond {111} surfaces.

1. For a collision energy E_i of 30 eV, the diamond surface is a more efficient activator of the peptide's internal modes, transferring ~20% of E_i to peptide vibration/rotation, while the SAM only transfers about 8%. In other recent work,[39,64] the diamond surface is also found to be a more efficient activator of $Cr(CO)_6^+$ projectile ions than is the SAM surface.

2. For 30-eV collisions with the diamond surface, the energy-transfer probabilities are similar for folded and extended structures of $(Gly)_3$. However, for collisions with the SAM surface, energy transfer to the peptide's internal modes does not depend on its structure, but energy transfer to the surface vibrations and translation of the scattered projectile depends on the peptide's structure. Energy transfer to E_{surf} and E_{int} is 9% smaller and larger, respectively, for the extended structure. This is an interesting finding, which is clearly related to experimental studies of the influence of secondary structure on the fragmentation of peptides[13,68] and needs further investigation. The effect of different energy-transfer distributions, for different peptide structural conformations, would be to broaden energy-transfer distributions for experimental studies, in which the projectile ion beam is composed of a distribution of structural conformations.

3. Constraining various modes of folded $(Gly)_3$ shows that ~80% of the energy transfer to the peptide's internal modes goes to the torsions. That the peptide torsions are the principal "accepting modes" of energy in SID agrees with the ~84% transfer of internal energy to peptide torsions in a recent simulation of peptide CID.[40]

(66) Shin, H. K. In *Dynamics of Molecular Collisions, Part A*.; Miller, W. H., Ed.; Plenum: New York, 1976; p 131.
(67) Yardley, J. T. *Introduction to Molecular Energy Transfer*; Academic Press: London, 1980.
(68) Tsaprailis, G.; Nair, H.; Somogyi, A.; Wysocki, V. H.; Zhang, W.; Futrell, J. H.; Summerfeld, S. G.; Gaskell, S. J. *J. Am. Chem. Soc.* **1999**, *121*, 5142.

4. The percent energy transfer to the peptide's internal modes is only weakly dependent on peptide size. For folded $(Gly)_3$ colliding with the diamond surface, 18% of the collision energy is transferred to E_{int}, while this energy transfer is 23% for folded $(Gly)_5$. This small increase in energy transfer to E_{int}, for $(Gly)_5$ collisions with the diamond surface, comes at the expense of energy transfer to the surface vibrations.

5. The partitioning of the energy transfer, between the projectile's internal modes E_{int}, the surface vibrations E_{surf}, and projectile final translation E_f depends on the collision energy E_i. For folded $(Gly)_3$ collisions with diamond {111}, percent energy transfer to E_{int} first increases with E_i and then decreases. Energy transfers to E_{surf} and E_f increase and decrease, respectively, with increase in E_i. Similar patterns in collisional energy transfer were found in recent simulations of $Cr(CO)_6^+$.[64]

6. For the same surface and collision energy, more of the collision energy is transferred to the internal modes of $Cr(CO)_6^+$ than to internal modes for either $(Gly)_3$ or $(Gly)_5$, though the latter have more internal degrees of freedom. The efficiency of internal energy transfer depends in part on the number of modes that can act as active pathways for receiving the collision energy. This work and that reported earlier[38] indicate that only the torsions of the peptides are efficient receptors of the collision energy, while for $Cr(CO)_6^+$, only the CO stretches have been identified as inefficient energy-transfer pathways.

The $E_i \rightarrow E_{int}$ energy transfers found here for $(Gly)_3$ and $(Gly)_5$ colliding with the *n*-hexyl thiolate self-assembled monolayer (H-SAM) and diamond {111} surfaces are overall consistent with experiments by Laskin et al.[14] of dialanine SID on a fluorinated self-assembled monolayer (F-SAM) surface consisting of the FC_{12} alkanethiol $CF_3(CF_2)_9\,C_2H_4SH$. However, it should be noted that in their collisions the projectile ion collisions are normal to the surface, instead of the 45° collision angle simulated here, and their distributions of $P(\Delta E_{int})$, which they describe as arising from a thermalization process, are broader than the ones reported here. Using RRKM modeling of the experimental results, Laskin et al. found that for a collision energy E_i in the 3−23-eV range on average 21% of E_i is converted to peptide internal energy E_{int}. For the simulations reported here, of folded $(Gly)_3$ colliding with the diamond {111} surface, the $E_i \rightarrow E_{int}$ energy transfer varies from 8 to 18% for E_i in the range of 10−110 eV, with a peak in the energy transfer of ∼18% at E_i of ∼30 eV. For folded $(Gly)_3$ colliding with the softer H-SAM surface, the $E_i \rightarrow E_{int}$ energy transfer from the simulations is much smaller and 7% of E_i at 30 eV.

Previous work[69] has shown that $E_i \rightarrow E_{int}$ energy transfer is ∼5−10% larger for projectiles colliding with a F-SAM as compared to a H-SAM surface. There are several reasons why energy transfer to the projectile's internal modes is more important for collisions with a F-SAM. Because C−F bonds are longer than C−H bonds and the F-atom larger than the H-atom, repulsive forces between the alkyl chains will be more pronounced for the F-SAM, giving rise to a stiffer surface. In addition, the intermolecular potential between the projectile and the F-SAM may give rise to more energy transfer. The $E_i \rightarrow E_{int}$ energy transfer for peptide ions colliding with F-SAM surfaces is apparently similar to that for projectiles colliding with the diamond {111} surface. In future trajectory simulations, it will be important to study the SID of peptide ions colliding with F-SAM surfaces.

Acknowledgment. This research was supported by the National Science Foundation. The authors acknowledge important discussions with Luke Hanley, Julia Laskin, Graham Cooks, and Zdenek Herman.

JA011987N

(69) See ref 14 and references therein.